Construction and Building Materials 174 (2018) 173–189

Contents lists available at ScienceDirect

Construction and Building Materials

journal homepage: www.elsevier.com/locate/conbuildmat

COST TU1404 benchmark on macroscopic modelling of concrete and concrete structures at early age: Proof-of-concept stage

Agnieszka Jędrzejewska [a,*], Farid Benboudjema [b], Laurie Lacarrière [c], Miguel Azenha [d], Dirk Schlicke [e], Stefano Dal Pont [f], Arnaud Delaplace [g], José Granja [h], Karolina Hájková [i], Peter Joachim Heinrich [e], Giuseppe Sciumè [j], Emanuel Strieder [k], Elisabeth Stierschneider [k], Vít Šmilauer [i], Vyacheslav Troyan [l]

[a] Silesian University of Technology, Department of Structural Engineering, Gliwice, Poland
[b] LMT-Cachan/ENS-Cachan/CNRS/Université Paris Saclay, Cachan, France
[c] LMDC (Laboratoire Matériaux et Durabilité des Constructions), Université de Toulouse, INSA-UPS, Toulouse, France
[d] University of Minho, Department of Civil Engineering, Campus of Azurém, Guimarães, Portugal
[e] Graz University of Technology, Institut für Betonbau, Graz, Austria
[f] Université Grenoble Alpes, Grenoble, France
[g] Lafarge, Paris, France
[h] University of Porto, Porto, Portugal
[i] Czech Technical University in Prague, Prague, Czech Republic
[j] Institut de Mécanique et d'Ingénierie I2M, Université de Bordeaux, Bordeaux, France
[k] University of Natural Resources and Life Sciences, Institute of Structural Engineering, Vienna, Austria
[l] Kyiv National University of Construction and Architecture, Kyiv, Ukraine

HIGHLIGHTS

- Benchmark program to test models for thermo–mechanical macroscopic modelling of concrete.
- A proof-of-concept stage with simple examples of academic nature.
- Generalised conclusions for simulation of early-age behaviour of structural concrete.
- Thermal analysis: Impact of thermal activation and modelling of thermal boundary conditions.
- Mechanical analysis: impact of mechanical properties evolution and creep reproduction.

ARTICLE INFO

Article history:
Received 21 December 2017
Received in revised form 28 March 2018
Accepted 9 April 2018

Keywords:
Early-age concrete
Numerical modelling
Macroscopic modelling
Benchmark program

ABSTRACT

Modelling of early-age behaviour of cement-based materials is still a challenging task. The challenge is implied by the extent of the knowledge on the subject which results in a variety of different models used for simulation of cement-based materials. That is why a numerical benchmark program has been launched within the COST Action TU1404 aiming at improvement and harmonisation of computational prediction of early-age behaviour of cement-based materials as well as its behaviour on structural level. This paper presents the result of the proof-of-concept stage of the benchmark.

The goal of this stage of benchmark was to compare the performance of currently used models for simulation of early-age behaviour of concrete. The participants were requested to simulate thermo-chemo-mechanical behaviour of simple concrete elements covering adiabatic and real evolution of temperature, shrinkage, stiffness and stresses accounting for early-age creep. The tasks were formulated based on the experimental measurements. This stage of benchmark allowed to evaluate the influence of different phenomena occurring in early-age concrete on the behaviour of early-age concrete structures, define the discrepancies between experimental results and numerical simulations, as well as to indicate the weak points in the models.

* Corresponding author.
E-mail address: Agnieszka.Jedrzejewska@polsl.pl (A. Jędrzejewska).

https://doi.org/10.1016/j.conbuildmat.2018.04.088
0950-0618/

1. Introduction

Modelling of early-age behaviour of cement-based materials is still a challenging task. The challenge is not implied by little knowledge on the subject but – in contrary – by its extent. As a result, there is a variety of different models currently used for simulation of CBMs. A fundamental tool for assisting the development, understanding and comparison of the models are benchmarking tests. That is why a numerical benchmark program has been launched within the COST Action TU1404 [1], which first stage is presented in this paper. The aim of this benchmark is to improve and harmonise computational prediction of early-age behaviour of cement-based materials as well as its behaviour on structural level. The benchmarking program consists of three stages [2].

Stage 1, which has already been completed, was a proof-of-concept stage. It consisted of simple examples. The examples to be simulated were based mostly on the published experimental data and were fully open: the participants had access to all input data as well as final results. The simulations focused both on material properties and structural phenomena. In Stage 2, which is currently on-going, extended examples are studied. The main aim of this stage is to model the results of the COST Action TU1404 Extended Round-Robin Test (RRT$^+$) experiments [3]. The benchmark program will conclude with Stage 3 in which participants are invited to join EDF Vercors 2018 benchmark [4].

This benchmark program was inspired by similar initiatives such as [5]. The report of NAFEMS (International Association for the Engineering Modelling, Analysis and Simulation Community), published in 1986 was at that moment a state of the art on numerical solutions of thermal problems and provided a set of benchmark tests for numerical thermal analysis. However, because of significant development in numerical analysis since that time the report no longer represents current best practice. The proposed tasks cover only one and two-dimensional problems of general nature. That is why the organisers of the COST TU1404 benchmark came up with the idea to create a benchmark program dedicated to modelling of thermal problems in early-age concrete structures.

Stage 1 of the benchmark program based on the idea of the NAFEMS benchmark by providing a set of relatively simple tasks of academic nature which would be easy to model but still provide a test of the capability of the proposed models. This stage was subdivided into microscopic benchmarking focusing on prediction of pure material behaviour on microstructural level (please refer to [6] for details of this benchmark) and the herewith presented macroscopic benchmarking focusing on simulation of structural behaviour on the level of building components. Following a summarised presentation of the preliminary results of this benchmark in [7], the present paper focuses on a final, broader and detailed discussion of the completed benchmark. The aim of this stage was to provide (i) basic strategies for computational simulation of early-age behaviour of cement-based materials and structures as well as (ii) reference examples for validation of calculation models.

The participants were requested to simulate thermo-chemo-mechanical behaviour of simple concrete elements (including concrete cube and restrained frame experiment) covering adiabatic and real evolution of temperature, shrinkage, stiffness and restrained stresses accounting for early-age creep. The tasks were formulated based on the experimental measurements. The paper starts with detailed definition of the tasks, including description of the experiment, input data, formulation of the problem and expected output data. This section is followed by brief introduction and preliminary comparison of the models used by participants (thermal and mechanical models are presented separately since all the teams used uncoupled approach). Then, the results of simulations of the three tasks with the before presented models are shown and discussed. The main conclusions of the benchmark close the paper. This stage of benchmark allowed to evaluate the influence of different phenomena occurring in early-age concrete on the behaviour of early-age concrete structures, define the discrepancies between experimental results and numerical simulations, as well as to indicate the weak points in the models.

2. Benchmark program

The task was to perform thermo–chemo–mechanical calculations of the 3 prepared examples. 9 teams altogether have participated in the first stage of the benchmark as specified in Table 1. The following sections introduce in detail the tasks of the benchmark program. It must be emphasised that the experimental input data were obtained in single experiments, therefore variations of the measurements cannot be characterised neither their impact with respect to the precision of simulations.

2.1. Task 1: modelling of temperature and thermal stress development in a simple structure

The example was aimed at benchmarking macroscopic models simulating temperature and stresses evolution in simple structures. This task was purely numerical.

Table 1
Teams participating in tasks of the numerical benchmark program.

Modelling challenge:	TASK 1 temperature and elastic stress development (numerical) • Temperature • Shrinkage strain • Young modulus • Elastic stress	TASK 2 temperature development in a massive cube • Temperature	TASK 3 thermal stress in shrinkage restraining device • Temperature • Shrinkage strain • Young modulus • Viscoelastic stress (creep)
Team 1	x	x	x author of the task
Team 2	x	x	x
Team 3	x	x author of the task	x
Team 4		x	
Team 5	x		
Team 6	x		
Team 7		x	
Team 8	x author of the task		
Team 9	x		
Analysis of results	F. Benboudjema	L. Lacarrière	A. Jędrzejewska

As input data, concrete mix design, evolution of adiabatic temperature, thermal and mechanical properties (from experiments or generated) were provided. The participants were asked to:

1. Calibrate their models to properly reproduce evolutions of adiabatic temperature for two initial temperatures as well as of autogenous shrinkage and elastic properties.
2. Predict stresses in a Gauss point in homogeneous conditions (adiabatic and 3D restraint), see Fig. 1.

Constant material properties specified in the task are given in Table 2. Initial and boundary conditions for the numerical simulation are given in Table 3. The adiabatic temperature evolution is given in Fig. 2 for two initial temperatures. Evolutions of Young modulus and autogenous shrinkage at 20 °C are given in Fig. 3.

2.2. Task 2: modelling of temperature development in a massive concrete cube

The task was based on the publication by Azenha et al. [8]. The aim of this task was to test the capability of the models to simulate evolution of non-linear and non-stationary thermal fields in a concrete block cast and monitored within a climatic chamber. In this experiment the environmental and materials conditions were precisely controlled. This control of the boundary conditions allows comparing the efficiency of the material model by eliminating any discrepancy in the simulations results that can be due to the lack of knowledge in boundary conditions as it could be the case in real structures.

The simulated test was performed at the University of Porto. A concrete cube of 400 mm edge side was cast into a plywood formwork and cured inside a climatic chamber at ~20 °C temperature. At very early ages, the cube was confined on 5 surfaces by the formwork (one bottom and 4 lateral ones), whereas the top surface was kept exposed to the surrounding environment. The four lateral formwork panels were removed at the age of 8.6 h. Temperature evolutions were measured on the surfaces (thermography, see Fig. 4) and inside using thermocouples. For detailed information about measurements and positioning of temperature sensors, the reader is referred to [8].

The concrete used was made with CEM I cement; its composition is given in Table 4.

Thermal characteristics of the concrete and boundary conditions are given in Table 5 in order to ensure that the calculations can be compared with similar hypothesis. Indeed, the aim of this case study is not to test thermal transfer models but to see the influence of the heat release model on the thermal behaviour of a concrete element. It is relevant to say that the data found in Table 5 was obtained directly from [8], where a finite element simulation of the temperature development inside the cube was performed and successfully compared with the corresponding experimental data. The participants were also given results of isothermal calorimetry performed on the tested material in various temperatures (20, 30, 40, 50, 60 °C) to calibrate their thermal models (see Fig. 5).

Table 2
Material properties of concrete in task 1.

Property	Value	Unit
Volumetric thermal capacity	$2.4 \cdot 10^6$	J/(m^3·K)
Thermal conductivity	1.75	W/(m·K)
Poisson ratio	0.2	–
Coefficient of thermal expansion	10^{-5}	1/K

Table 3
Initial and boundary conditions in task 1.

Name	Value	Unit
Initial temperature	20	°C
Ambient temperature	20	°C
Coefficient of thermal exchange (convection and radiation after linearization)	10	W/(m^2·K)

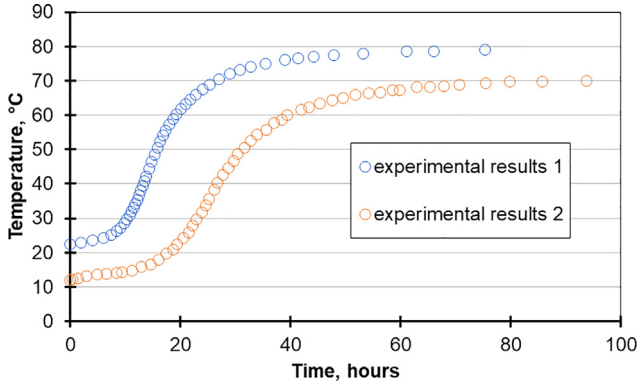

Fig. 2. Development of adiabatic temperature of concrete in task 1 for two distinct initial temperatures.

The teams were asked to provide temperature evolutions at 3 thermocouples locations from casting to 1 day. The locations of the sensors are specified in Fig. 6. One of the sensors (TP18) was located in the core of the cube, the other (TP9 and TP3) were located 5 cm beneath the lateral surface and respectively at mid-height (TP9) and at 5 cm from the lower face (TP3). Temperature evolutions in these locations are shown in Fig. 7.

2.3. Task 3: modelling development of thermal stress in shrinkage restraining device

The task was based on the publication by Turner et al. [9]. The aim of this task was to test the capability of the models to simulate

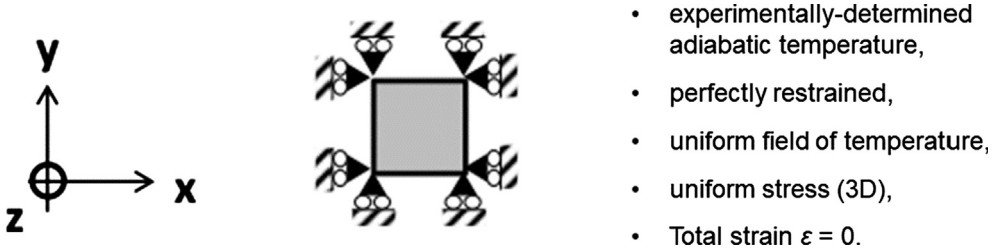

Fig. 1. Description of the geometry and boundary conditions for task 1.

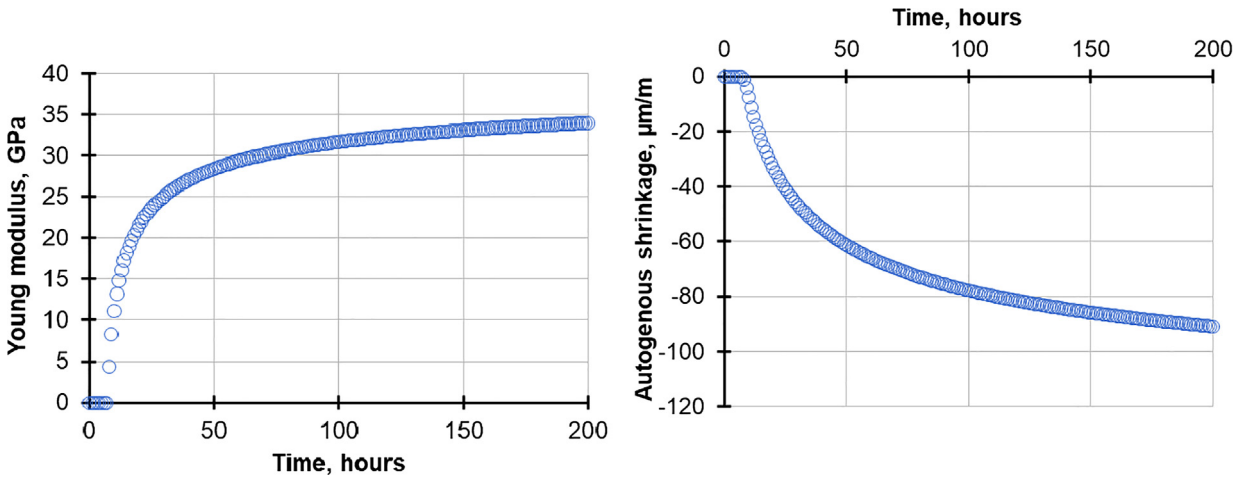

Fig. 3. Time-development of Young modulus (left) and autogenous shrinkage (right) in concrete of task 1 in isothermal conditions (20 °C).

Table 4
Mix composition of concrete used in the massive cube experiment.

Component	Amount	Unit
Cement (Type I 52.5R)	430	kg/m^3
Limestone filler	301.5	kg/m^3
Sand 1	339.7	kg/m^3
Sand 2	335	kg/m^3
Coarse aggregate	729.7	kg/m^3
Water	193.4	kg/m^3
Superplasticiser (liquid)	6.8	kg/m^3

development of stresses due to imposed shrinkage in externally-restrained conditions.

The simulated test was performed in the restraining frame designed and constructed at the Institute of Structural Concrete of Graz University of Technology, shown in Fig. 8. This testing set-up was developed for the experimental simulation of holistic restraint stress histories and crack developments in reinforced concrete members beginning from early age with continuous transition to service life, whereby the benchmark program concentrates at the current stage only on the early-age phase of one specimen without cracking.

The specimen had dimensions of 3.7 × 0.25 × 0.25 m and the temperature history of the hardening phase was solely induced by the material behaviour itself under a defined insulation without any artificial measures of heating or cooling. Thermal properties of insulation materials are given in Table 6.

The accompanying stress history resulted purely from the externally and passively restrained deformation behaviour due to temperature history according to hydration heat and treatment as well as shrinkage with respect to the evolution of Young modulus as well as viscoelastic material behaviour. At the end, the stiffness of the frame provides a restraining degree of 65% in the hardened and uncracked state of the considered specimen.

The concrete used in the experiment was an OPC of C35/45 class. Composition of the concrete mix is specified in Table 7. The thermo–mechanical characterisation of this concrete was made at iBMB TU Braunschweig [10] and it included adiabatic temperature and mechanical properties development in time. The adiabatic temperature curve for the analysed concrete is shown in Fig. 9 while all the relevant thermal properties of this concrete are collectively presented in Table 8. Mechanical properties are collectively presented in Table 9. The final value of shrinkage was given as 0.05‰.

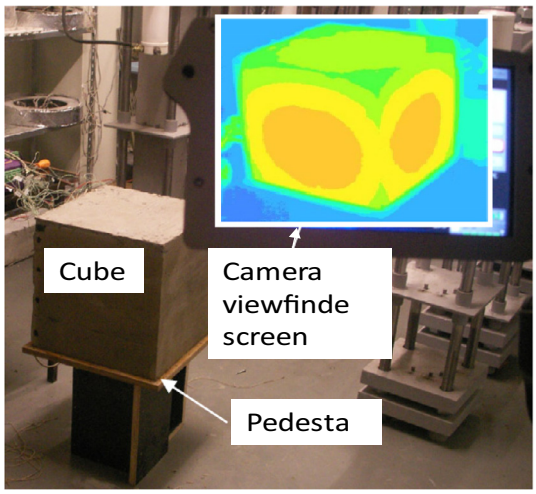

Fig. 4. Specimen and device for the measurement of temperature in the massive concrete cube by thermography, adopted from [8].

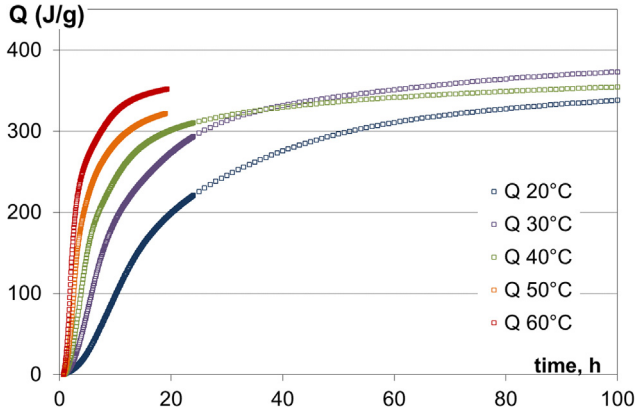

Fig. 5. Isothermal calorimetry curves for different temperatures in the massive concrete cube experiment.

The test was performed in the ambient temperature of 22 °C. Formwork was removed after 265 h of curing. Heat transfer coefficient was advised by the authors of the task as 10 W/(m^2·K) when the concrete was in formwork and 20 W/(m^2·K) for a free concrete

Table 5
Thermal properties of concrete used in the massive cube experiment after [8].

Property			Value	Unit
Concrete initial temperature			26	°C
Heat capacity			2400	kJ/(K·m^3)
Thermal conductivity			2.6	W/(K·m^3)
Climatic chamber temperature			20	°C
Surface convective coefficient	Top Boundary ("free" surface)		10	W/(K·m^2)
	Lateral Boundaries	From 0 h to 8.6 h (with formwork)	5.208	
		After 8.6 h ("free" surface)	10	
	Bottom Boundary (with formwork)		5.208	

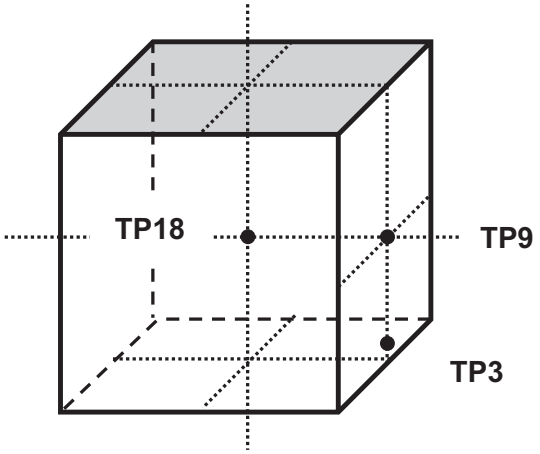

Fig. 6. Locations of sensors in the massive concrete cube experiment.

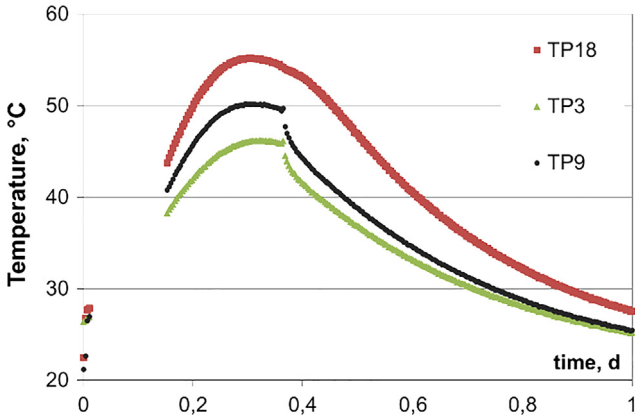

Fig. 7. Temperature evolution in chosen locations in the massive concrete cube experiment.

Table 6
Thermal properties of insulation materials used in the restraining frame experiment.

	Formwork	XPS	Unit
Conductivity	0.24	0.06	W/(m·K)
Volumetric heat capacity	1600	100	kJ/(m^3·K)

Table 7
Mix composition of concrete used in the restraining frame experiment.

Component	Amount	Unit
CEM III/A 32.5N Holcim	300	kg/m^3
Water	145	kg/m^3
Aggregates 0/16	2000	kg/m^3
BV ViscoCrete-1051 PCE	3	kg/m^3

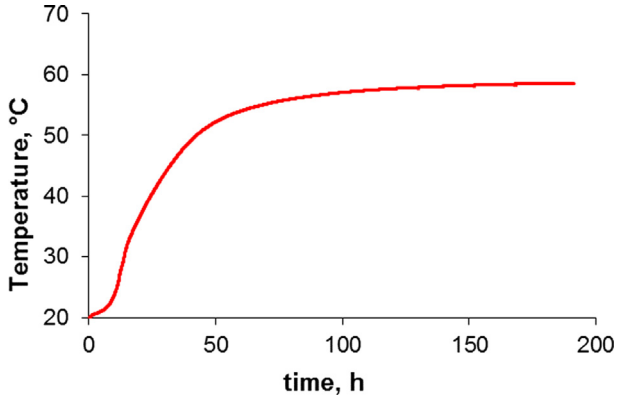

Fig. 9. Adiabatic temperature rise in concrete used in the restraining frame experiment.

surface, determined assuming heat exchange by convection and radiation and taking into consideration thermal properties of the covering material. Development of temperature, measured in the core and at the corner of the concrete specimen, is shown in Fig. 10 (left). The averaged measured stress in the specimen (as

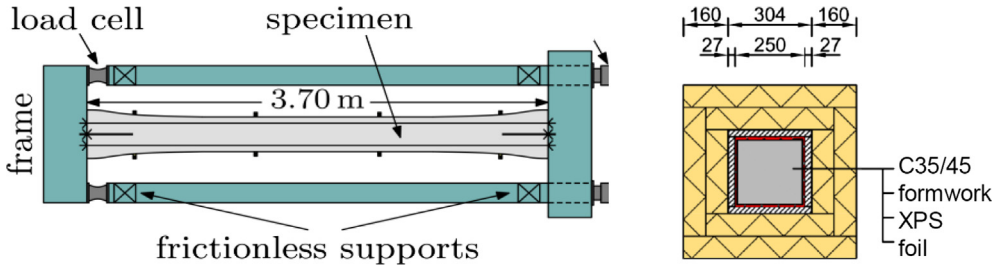

Fig. 8. Restraining frame set-up" top view (left) and cross-section (right).

Table 8
Thermal properties of concrete used in the restraining frame experiment.

Property	Value	Unit
Activation Energy[(1)]	46,000	J/mol
Setting time[(1)]	10.5	h
Heat capacity[(2)]	2500	kJ/(K·m^3)
Thermal conductivity[(2)]	2.4	W/(K·m^3)
Poisson's ratio[(2)]	0.2	–
Thermal expansion[(2)]	0.00001	1/K

(1) Measured value.
(2) Re-calculated value.

computed form load cell results and known cross-sectional dimensions of the specimen) in Fig. 10 (right).

The goal of this task was to simulate temperature and stress development in a restrained concrete sample as shown in Fig. 10.

3. Modelling strategies

The teams used different approaches to modelling development of temperature and stresses in early-age concrete elements. All the approaches, however, were macroscopic approaches implemented in the FEM-based computer codes. This section introduces the modelling challenges and briefly presents the models used by the teams to simulate the phenomena in question.

3.1. Temperature evolution (Thermo–chemical models)

Computation of thermal fields in concrete was made by all teams by solution of the heat balance equation:

$$\lambda \nabla \cdot (\nabla T) + \dot{Q} = \rho c \dot{T} \tag{1}$$

where:
λ – thermal conductivity, W/(m·K);
ρ – density, kg/m^3;
c – specific heat capacity, kJ/(kg·K);
$\dot{Q}$ – hydration heat development rate, J/(m^3·s);
T – temperature, K.

Thermal properties of concrete were always taken as constant in time and the associated boundary conditions were modelled by a heat flux $\tilde{q}$ across the boundaries:

$$\tilde{q} = h(T_b - T_a) \tag{2}$$

where:
h – heat transfer coefficient, W/(m^2·K). Heat exchange by convection and radiation (after linearization) was considered expressed with a single coefficient taking also into account the effect of covering materials (whenever relevant);
T_a – ambient temperature, °C (K);
T_b – temperature at the boundary, °C (K).

The teams used different functions for modelling heat generation.

Teams 1 and 9 used an equivalent time approach for the heat generation function (t_{eq} after [11]):

$$t_{eq} = \int \exp\left\{\frac{A}{R} \cdot \left[\frac{1}{293} - \frac{1}{273 + T(t)}\right]\right\} dt$$

with $A = \max\{E_a; E_a + 1470 \cdot (20 - T(t))\}$where: E_a/R – activation energy, 1/K.

Team 1 Heat generation function after [12]:

$$Q(t) = Q_{max} \cdot \exp\left\{b \cdot \ln\left(1 + \frac{t_{eq}}{\tau_k}\right)^a\right\}$$

where:
Q_{max} – theoretical value of the total hydration heat with respect to the end value of the form function reached by the parameter set, J/m^3;
a, b, τ_k – fitting parameters.

Table 9
Mechanical properties of concrete used in the restraining frame experiment.

Time [days]	$f_{cm}(t)$ [MPa]	$E_{cm}(t)$ [MPa]	$E_{ct}(t)$ [MPa]	$f_{ctm}(t)$ [MPa]
1	6.6	–	–	–
2	15.5	19,633	26,700	1.55
3	19.9	–	–	–
4	24.1	25,933	31,400	–
7	36.7	30,450	35,600	2.90
14	44.7	34,100	–	3.33
28	57.8	34,133	41,300	3.90
56	58.8	–	–	–

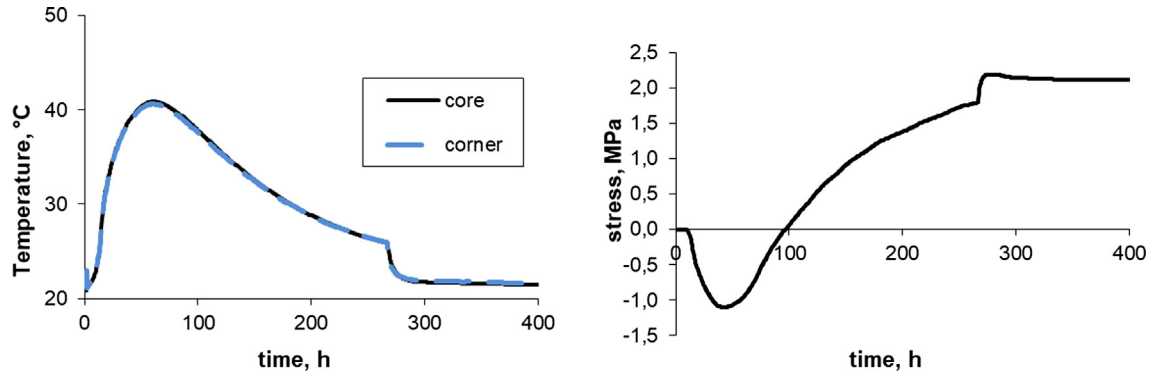

Fig. 10. Time-development of temperature (left) and average stress (right) in concrete specimen in the restraining frame experiment.

Team 9 Heat generation function with parameters fitting acc. to [13]:

$$Q(t) = \frac{\alpha_Q \cdot Q_\infty \cdot fac_Q \cdot c \cdot \tau_{e,Q} \cdot \exp\left[-\left(\frac{\tau_{e,Q}}{t_{eq}}\right)^{a_Q}\right] \cdot \left(\frac{\tau_{e,Q}}{t_{eq}}\right)^{a_Q - 1}}{t_{eff}^2} + \frac{\alpha_{Q2} \cdot Q_\infty \cdot (fac_Q - 1) \cdot c \cdot \tau_{e,Q2} \cdot \exp\left[-\left(\frac{\tau_{e,Q2}}{t_{eq}}\right)^{a_{Q2}}\right] \cdot \left(\frac{\tau_{e,Q2}}{t_{eq}}\right)^{a_{Q2} - 1}}{t_{eq}^2}$$

where:

Q_∞ – total hydration heat, J/m^3;
c – amount of cement in the mix, kg/m^3;
$\tau_{e,Q}$, $\tau_{e,Q2}$ – fitting parameters, h;
a_Q, a_{Q2}, fac_Q – fitting parameters, [–].

Teams 2 and 7 used the affinity approach for the heat generation function based on the degree of hydration:

$$\dot{Q} = \dot{\alpha} \cdot Q_{pot} = Q_{pot} \cdot \tilde{A}_{ref}(\alpha) \cdot \exp\left(-\frac{E_a}{RT}\left(\frac{1}{T} - \frac{1}{T_{ref}}\right)\right) \quad (3)$$

where:

Q_{pot} – total hydration heat for a theoretical complete hydration, J/m^3;
E_a/R – activation energy, 1/K;
T – concrete temperature, K;
T_{ref} – reference temperature used for determination of $\tilde{A}_{ref}$ [K];
$\tilde{A}_{ref}$ – affinity law, 1/s.

Team 2 Affinity law after [14]:

$$\tilde{A}_{25}(\alpha) = B_1\left(\frac{B_2}{\alpha_{max}} + \alpha\right)(\alpha_{max} - \alpha)\exp\left(-\eta\frac{\alpha}{\alpha_{max}}\right)$$

where:

$\tilde{A}_{25}$ – chemical affinity at 25 °C, 1/s;
α and α_{max} – degree of hydration and ultimate degree of hydration, [–];
B_1, B_2 – fitting parameters; 1/s, [–];
η – microdiffusion of free water through formed hydrates, [–].

Team 7 Affinity law after [15]:

$$\tilde{A}_{T_{ref}} = K \cdot \frac{\alpha \cdot C_{c0}}{W} \cdot \exp\left[-\frac{1}{n} \cdot \left(\frac{1}{r_k} \cdot \frac{\alpha}{(1-\alpha)} \cdot \frac{R_{Vh/a}}{W \cdot \phi}\right)^n\right]$$

where:

$\tilde{A}_{T_{ref}}$ – chemical affinity at the reference temperature, 1/s;
K – global kinetic constant, 1/s;
n, r_k – fitting parameters, (dimensionless);
W – water content in the paste, m^3/m^3;
ϕ – porosity of the paste, m^3/m^3;
C_{c0} – initial cement content in the paste, m^3/m^3;
$R_{Vh/a}$ – represent the volume of hydrates produced by the hydration of 1 m^3 of anhydrous cement, m^3 hydrates/m^3 anhydrous cement reacting.

Teams 3, 5, 6 and 8 also used the affinity approach for the heat generation function but based on the degree of reaction:

$$\dot{Q} = \dot{r} \cdot Q_{max} = Q_{max} \cdot \tilde{A}_{ref}(r) \cdot \exp\left(-\frac{E_a}{RT}\left(\frac{1}{T} - \frac{1}{T_{ref}}\right)\right) \quad (4)$$

where:

Q_{max} – maximal hydration heat at the end of the test, J/m^3;
E_a/R – activation energy, 1/K;
T – concrete temperature, K;
T_{ref} – reference temperature used for determination of $\tilde{A}_{ref}$ [K].

Teams 3, 5, 6 and 8 Affinity law after [16]:

$$\tilde{A}_{20}(r) = Af(r)\exp\left(-\frac{E_a}{293 \cdot R}\right)$$

where:

$\tilde{A}_{20}$ – chemical affinity at a reference temperature of 20 °C, 1/s;
A – rate constant, J/s·m^3;
r – degree of reaction considered as the ratio between the heat Q released up to time t and the total heat Q_{max} released at the end of the test;
$f(r)$ – normalised function for heat identify on isothermal calorimetry or (semi-) adiabatic tests.

Finally, Team 4 used a simpler approach by neglecting the thermal activation of hydration kinetic.

Team 4 Time-dependant heat generation function [17]:

$$Q(t) = Q_{max}(1 - \exp(-k \cdot t^n))$$

where:

Q_{max} – theoretical value of the total hydration heat with respect to the end value of the form function reached by the parameter set, J/g;
t – age of concrete, hours;
k, nq – fitting parameters, [–].

3.2. Thermal–shrinkage stress evolution (mechanical models)

Stress calculations were made in tasks 1 and 3, so the presented mechanical models are limited to the teams who participated in these tasks.

In all the approaches thermal strains were treated as imposed volumetric strains and computed based on the pre-determined temperature change:

$$\varepsilon_T = \alpha_T T \mathbf{1}$$

where:

α_T – thermal dilation coefficient, 1/K; constant value has been applied by all teams.
$\mathbf{1}$ – a unit tensor.

Analogically, shrinkage strains were also modelled as imposed isotropic free strains. Shrinkage strains were limited to autogenous shrinkage. The teams used different functions to model autogenous shrinkage, although all of them were related to heat release (expressed with the equivalent age of concrete, t_{eq}). Teams 4 and 7 participated only in task 2 where no mechanical analysis was performed so they are not presented in the following list.

Team 1

$$\varepsilon_{ca}(t) = \frac{\varepsilon_{ca,\infty}}{\alpha_{max}} \cdot \exp\left\{b \cdot \ln\left(1 + \frac{t_{eq}}{\tau_k}\right)^a\right\}$$

where:

α_{max} – maximum degree of hydration, [–];
$\varepsilon_{ca,\infty}$ – ultimate value of autogenous shrinkage strain, μm/m;
t_{eq} – equivalent age of concrete, h;
a, b, τ_k – fitting parameters. [–], [–], h;

Team 2

$$\varepsilon_{ca}(t_{eq}) = \varepsilon_{ca,\infty} \cdot \left[1 + \left(\frac{\tau_{au}}{t_{eq}}\right)^{w/c/0.38}\right]^{-4.5}$$

where:

(continued on next page)

$\varepsilon_{ca,\infty}$ – ultimate value of autogenous shrinkage strain, μm/m;
t_{eq} – equivalent age of concrete, days;
$\tau_{au} = (\frac{w}{0.38})^3$ with w/c being the water-to-cement ratio;

Team 3 The autogenous shrinkage obtained experimentally was introduced directly into the model (with linear interpolation).

Team 5 The autogenous shrinkage is taken proportional to the hydration degree.

Team 6 The autogenous shrinkage is calculated using the framework of unsaturated porous media, introducing capillary pressure, Biot coefficient, evolution of desorption isotherm with respect to hydration degree, see [18].

Team 8 $\varepsilon_{ca}(t) = \varepsilon_{ca,28}\left[\exp\left\{s\left(1-\sqrt{\frac{28}{t_{eq}-t_0}}\right)\right\}\right]^n$

where:
$\varepsilon_{ca,28}$ – value of autogenous shrinkage strain at 28 days, μm/m;
t_{eq} – equivalent age of concrete, days;
t_0 – equivalent setting time of concrete, days;
s, n – fitting parameters. [–], [–].

Team 9 $\varepsilon_{ca}(t_{eq}) = \varepsilon_{ca,\infty}\cdot\exp\left[-\left(\frac{\tau_{e,ca}}{\max(t_{eq}-t_{solidify};1/t_{solidify})}\right)^{a_{ca}}\right]$

$\varepsilon_{ca,\infty}$ – ultimate value of autogenous shrinkage strain, μm/m;
t_{eq} – equivalent age of concrete, h;
$t_{solidify}$ – effective time at solidification, h;
$\tau_{e,ca}$ – fitting parameter, h;
a_{ca} – fitting parameter, [–].

Stress development was determined with elastic approach and then assuming creep (viscoelastic models were applied). Detailed information about the models are collectively presented in the following table (Teams 4 and 7 participated only in task 2 where no mechanical analysis was performed):

Team 1 Stiffness (Young modulus) evolution with function after [19]:

$E_c(t) = E_{cm}\cdot[\exp\{-a\cdot w/c\cdot(t_{eq}^{\beta_{wes}} - 28^{\beta_{wes}})\}^{-1/3}]$

where:
E_{cm} – final value of the mean modulus of elasticity, GPa;
a, β_{wes} – fitting parameters, [–], [–];
w/c – water/cement ratio, [–];
t_{eq} – equivalent age of concrete, days.

Creep function taken according to [2] (basic creep only), modified after [20]:
asymmetric creep in tension and compression: $\varphi_{\infty,t} = 0.3\cdot\varphi_{\infty,c}$
modification of exponent in $\beta_c(t-t_0)$ with 0.17 instead of 0.3
non-linear creep under tension following [19]:
if $\sigma_c > 0.8 f_{ctk,0.05}$ creep coefficient is modified by $\varphi_{NL} = \varphi\cdot\exp\left\{1.5\cdot(\frac{\sigma_c}{f_{ct}(t)} - 0.45)\right\}$

Team 2 Stiffness evolution (Young modulus) according to B3 model from concrete composition [22].
Creep according to according to B3 model from concrete composition [22].

Team 3 Stiffness (Young modulus) evolution obtained experimentally was introduced directly into the model.
Creep was modelled with aging Kelvin chains. The parameters were obtained by fitting a DPL curve fitted to the given experimental data.

Team 5 $E(t) = E_\infty\overline{\alpha}^\beta$ with $\overline{\alpha} = \langle\frac{\alpha-\alpha_0}{\alpha_\infty-\alpha_0}\rangle_+$ after [23]

where:
α – degree of hydration, [–];
E_∞ – maximum value of Young modulus, GPa;
α_0 – percolation threshold, [–];
α_∞ – maximum degree of hydration, [–];
β – fitting parameter, [–].

1-stage Granger's creep model has been used, see [24].

Team 6 $E(t) = E_\infty\overline{\alpha}^\beta$ with $\overline{\alpha} = \langle\frac{\alpha-\alpha_0}{\alpha_\infty-\alpha_0}\rangle_+$ after [21]

where:
α – degree of hydration, [–];
E_∞ – maximum value of Young modulus, GPa;
α_0 – percolation threshold, [–];
α_∞ – maximum degree of hydration, [–];
β – fitting parameter, [–].

A Kelvin-Voigt model which parameters depend on the hydration degree has been used, see [18], after [23].

Team 8 $E_c(t) = E_{cm,28}\left[\exp\left\{s(1-\sqrt{\frac{28}{t_{eq}-t_0}})\right\}\right]^n$

where:
$E_{cm,28}$ – value of Young modulus at 28 days, GPa;
t_{eq} – equivalent age of concrete, days;
t_0 – equivalent setting time of concrete, days;
s, n – fitting parameters. [–], [–].

A Burger model (Kelvin-Voigt + Maxwell in series) which parameters depend on the hydration degree, equivalent time and temperature has been used, see [25].

Team 9 Stiffness (Young modulus) evolution with parameter fitting acc. to [11] and [26]:

$E(t_{eff}) = E_\infty\cdot\exp\left[-\left(\frac{\tau_{e,E}}{\max(t_{eff}-t_{solidify};1E-10)}\right)^{a_E}\right]$

where:
E_∞ – maximum value of Young modulus, GPa;
$t_{solidify}$ – effective time at solidification, h;
$\tau_{e,E}$, – fitting parameter, h;
a_E – fitting parameter, [–].

An empirical function was used to describe the creep behaviour for every loading increment in every time increment after [20,27]:

$\varepsilon_{creep}(t) = \varepsilon_{creep,\infty}\cdot\exp\left[-\left(\frac{\tau_{e,creep}\cdot t_0}{t_{eq}-t_0}\right)^{a_{creep}}\right]$

$d\varepsilon_{creep}(t) = \frac{\varepsilon_{creep,\infty}\cdot a_{creep}\cdot\exp\left[-\left(\frac{\tau_{e,creep}\cdot t_0}{t_{eq}-t_0}\right)^{a_{creep}}\right]\cdot\left(\frac{\tau_{e,creep}\cdot t_0}{t_{eq}-t_0}\right)^{a_{creep}}}{t_{eq}-t_0}$

where:
$\varepsilon_{creep,\infty}$ – ultimate value of creep, μm/m/MPa;
$\tau_{e,creep}$, a_{creep} – fitting parameters, [–];
t_0 – time at loading, h.

Table 10
Software used for simulations of the massive concrete wall.

	Team 1	Team 2	Team 3	Team 5	Team 6	Team 8	Team 9
Software used	SOFiSTiK	OOFEM [14]	DIANA	Code_Aster	Cast3m [18]	Cast3m [28]	Abaqus 2017 + Intel Fortran Compiler

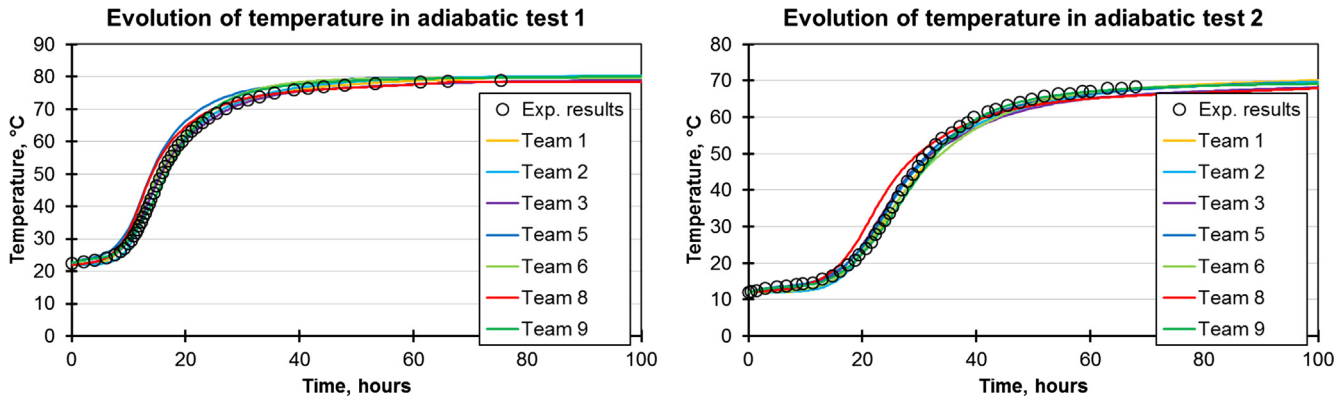

Fig. 11. Results of parameters identification on adiabatic calorimetry for 2 different initial temperatures in task 1.

Table 11
Parameters for thermal activation used in simulation of the two adiabatic tests.

Team 1	Team 3	Team 5	Team 8
$Q_{\infty t} = 145 \cdot 10^6$ [J/m^3] $E_a/R = 4029$ [1/K]	$E_a/R = 4510$ [1/K]	$E_a/R = 5402$ [1/K]	$Q_{\infty t} = 175 \cdot 10^6$ [J/m^3] $E_a/R = 5081$ [1/K]

4. Results and discussion

4.1. Task 1: Modelling of temperature and thermal stress development in a simple structure

4.1.1. General information on modelling approach

Detailed information on the modelling tools are collectively presented in Table 10.

4.1.2. Parameters identification: hydration and heat

Adiabatic calorimetry curves for two initial temperatures (results come from [29]) were given and allowed the teams to identify activation energy, heat release and hydration rate parameters.

All the teams took into account thermo-activation of the hydration process and were able to reproduce quite correctly the rise of adiabatic temperature for 2 different initial temperatures (see Fig. 11). Therefore, any differences for the next simulations should come from the mechanical models.

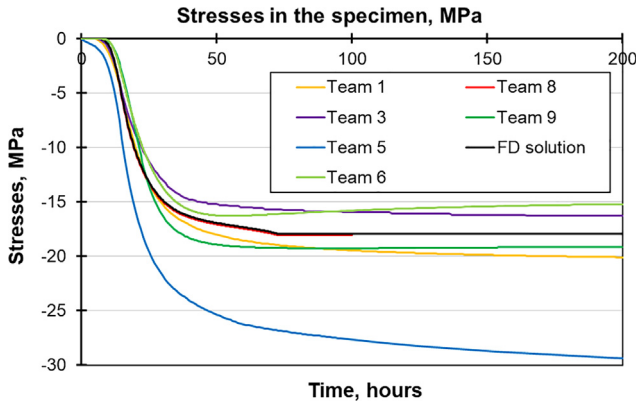

Fig. 13. Task 1: Time-development of stresses (creep is not considered) in adiabatic (initial temperature of 20 °C) and full restraint conditions.

For Teams 1, 3, 5 and 8, the activation energy is given in Table 11. It may be surprising that a wide range of activation energies has been found by inverse analysis (4029–5402 K^{-1}) although a good fit has been obtained for the adiabatic temperature.

4.1.3. Parameters identification: autogenous shrinkage and Young modulus

Prediction of stresses evolution in massive concrete structures depends highly on the prediction of temperature, but also Young modulus and autogenous shrinkage (amplitude and kinetic).

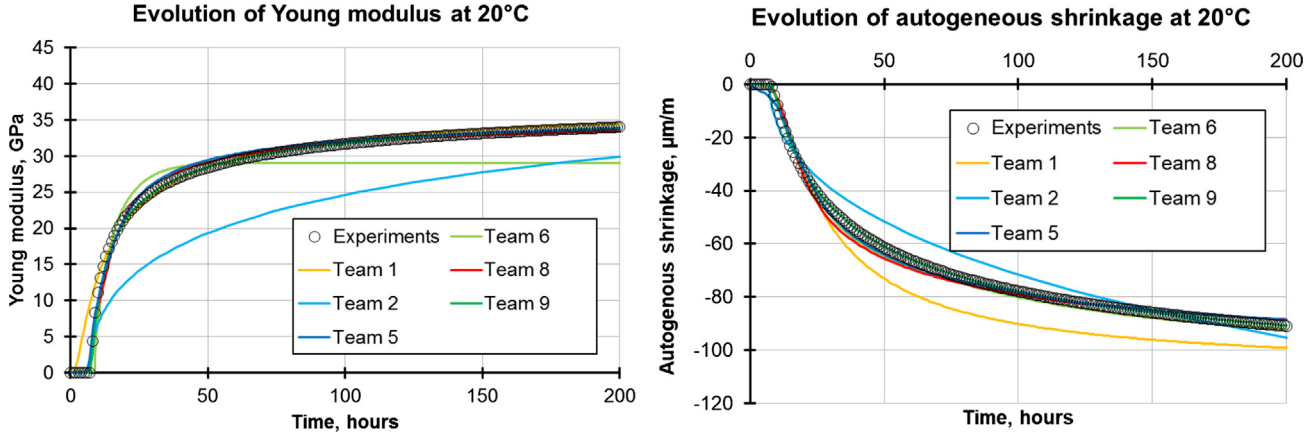

Fig. 12. Results of parameter identification on Young modulus and autogenous shrinkage (Team 3 is not reported since they used experimental evolution as input data).

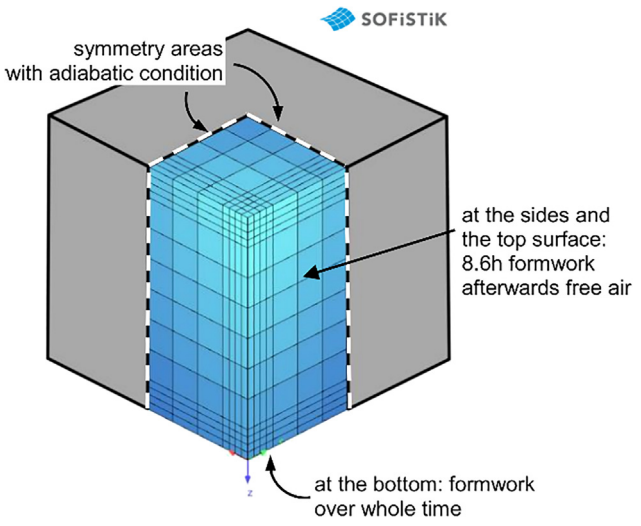

Fig. 14. FE models of the massive concrete cube experiment of Teams 1, 2, 3 and 7 based on the model of Team 1 (different meshing used by the teams).

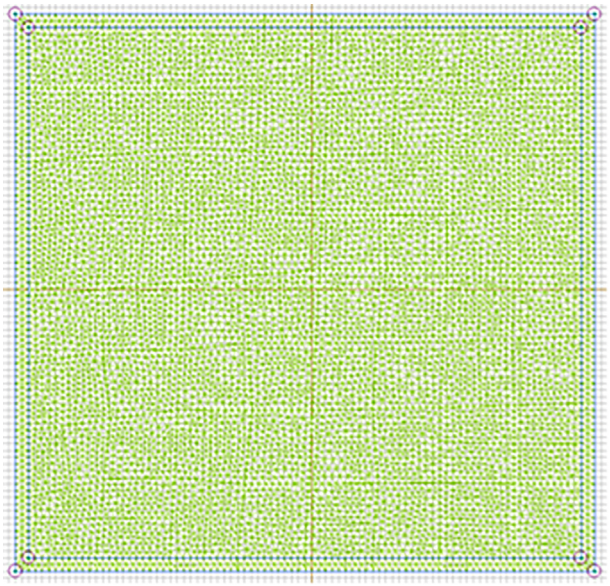

Fig. 15. 2D FE model of the massive concrete cube (formwork over whole time) experiment of Team 4 (meshing step 5 mm).

As it can be seen in Fig. 12, depending on the adopted model, some teams were not able to properly reproduce the evolution of Young modulus and/or autogenous shrinkage with respect to time at 20 °C (Teams 2 and 6 for the Young modulus; Teams 1 and 2 for the autogenous shrinkage). Besides, Team 1 did not assume a zero Young modulus before the setting time, which could lead to the rise of stresses too rapidly. Therefore, for the further comparison regarding stresses, Teams' 1, 2 and 6 contribution should be regarded carefully.

4.1.4. Results of the case study

This case study (see Fig. 1) considers homogenous state of temperature, strain and stress. 3D calculations in full restraint conditions with adiabatic temperature rise are considered (initial temperature of 20 °C). Finite difference (FD) solution can be obtained (parameters fitting of Team 8 has been used) and will be compared to the results of other teams, in the case when creep is not considered.

The stresses evolutions are given in Fig. 13 and include the results of numerical simulations performed by the teams compared with the Finite Difference solution (creep is not considered).

About 5 MPa of maximal differences is obtained between the teams (except for Team 5 who predicts too much compressive stresses), although some scattering has been observed regarding the reproduction of the Young modulus and autogenous shrinkage evolutions. Team 6 proposed too rapid plateau for the Young modulus, lower than reference values, which is consistent with the lower predicted value of compressive stresses. However, Team 1 predicted too large value of autogenous shrinkage, which is not consistent with higher value of predicted compressive stresses.

4.2. Task 2: modelling of temperature development in a massive concrete cube

4.2.1. General information on modelling approach

Detailed information on the modelling tools and assumptions for FE models are collectively presented in Table 12.

4.2.2. Parameters identification

Isothermal calorimetry curves at different temperatures were given and allowed the teams to identify activation energy and kinetic model parameters for Teams 1, 2 and 7, the activation energy and the affinity law for Team 3, and the kinetic model parameters for Team 4 (see Table 13).

The results of the fitting for all teams are given in Fig. 16. Several remarks can be made on the fitting made by different teams.

As Team 4 did not consider thermal activation, the heat development is the same for all temperatures. Team 4 decided to fit their kinetic parameters on the one observed at 30 °C ad 40 °C. We will see on the cube temperature that this choice was guided by the fact that the temperature observed in the cube was around 40 °C between 3 h and 8 h when the kinetic was high.

Teams 1, 2, 3 and 7 give quite similar results, with an "equivalent time approach" for Team 1, and with a "hydration (or reaction) degree approach" for Teams 2, 3 and 7. For Team 2 we can observe an overestimation of the heat released for the test at 60 °C after 12 h. This would be without consequences on the application to the cube presented in Section 4.2 because after 12 h the temperature in the cube is mainly governed by the cooling through the surfaces (as it can be observed in Figs. 18 and 19).

Teams 2, 3 and 7 used an affinity law based on hydration degree but some differences can be noticed on the results of isothermal calorimetry. Results obtained by Team 3 for 60 °C are slightly

Table 12
Details of numerical simulations of the massive concrete cube experiment.

	Team 1	Team 2	Team 3	Team 7	Team 4
Software used	SOFiSTiK	OOFEM [14]	DIANA	Cast3m [30]	ELCUT (QuickField)
FE idealisation	• regularly meshed 8-node volume elements • thermal boundaries over 2D elements at the surfaces • ¼ of the specimen (double symmetry)				• 2D model
	see Fig. 14				see Fig. 15

Table 13
Parameters for kinetic law and thermal activation used in simulation of the massive cube experiment.

Team 1	Team 2	Team 3	Team 4	Team 7
Q_{max} = 440 [J/g]	Q_{pot} = 500 [J/g]	Q_{max} = 383 [J/g]	Q_{max} = 315 [J/g]	Q_{pot} = 450 [J/g]
E_a/R = 5713 [1/K]	E_a/R = 5653 [1/K]	E_a/R = 5715 [1/K]	n = 2	E_a/R = 5000 [1/K]
a = -2.25	B_1 = 0.0002916 [1/s]	A = 1.21·10^6 [J/(s·g)]	k = 0.02	K = 3.16·10^4 [1/s]
b = -6.15	B_2 = 0.0024229	and $f(r)$ identified by inversed analysis		r_k = 2.00
τ_k = 6480 [s]	α_{max} = 0.875			n = 0.24
	η = 5.554			$R_{Vh/a}$ = 1.85

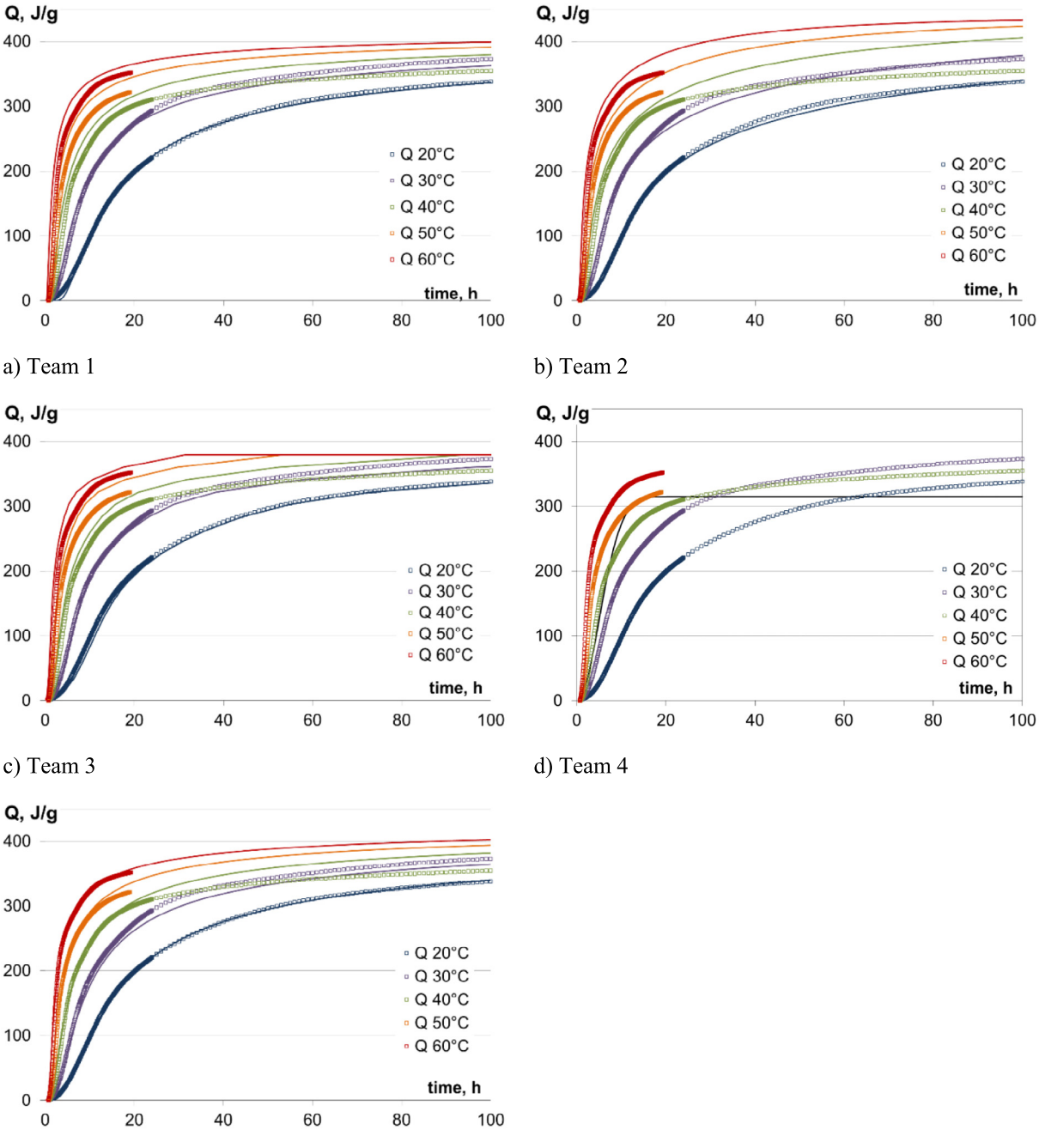

Fig. 16. Results of parameter identification on isothermal calorimetry for massive concrete cube simulation.

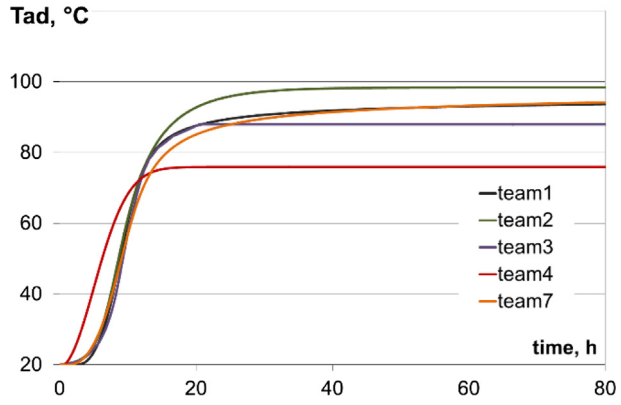

Fig. 17. Adiabatic temperature evolution predicted by the model for the same concrete as used in the massive cube experiment (assumed initial concrete temperature of 20 °C).

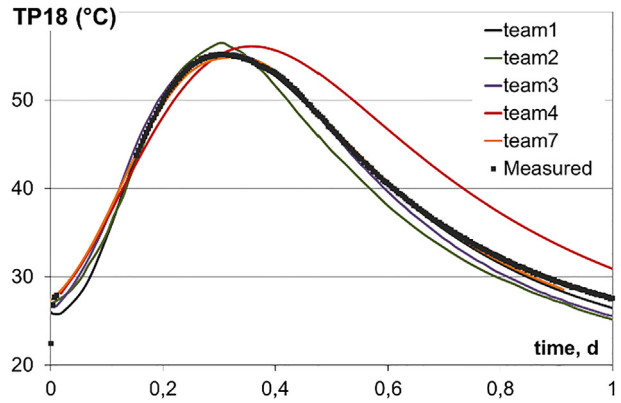

Fig. 18. Core temperature from casting to 1 day in a massive concrete cube.

different from Team 7, who also use the affinity approach, because the hydration is suddenly stopped (by reaching the maximal value of the reaction degree) around 25 h after casting. It must be noticed first that for Team 3 r is the reaction degree which reaches 1 at the end of the reaction. For Teams 2 and 7, α is the hydration degree which reaches the maximal value (depending on the w/c ratio, among the others) when the reaction is stopped. For the test reproduced here, the maximal value is not reached by the simulation of Teams 2 and 7 (whatever the temperature of the test) which traduces the fact that it is considered still enough water for the reactions to continue after 100 h. Regarding as the W/C ratio of the binder used (0.45) it seems coherent to have a continuation of reactions after 100 h even at 60 °C.

4.2.3. Results of the adiabatic simulation

To first observe the effect of the differences in the fitting results on an idealised case, we can calculate with each model the temperature evolution in an adiabatic case (totally insulated structure) which is the maximal temperature that could be obtained with this concrete formulation. The results are presented in Fig. 17.

In this case study (purely numerical because no adiabatic calorimetry results were available for this concrete) the influences of the difference between the models and of calibration choices made by the teams are emphasised.

First, for the results of Team 4 who did not take into account thermal activation, the approximate calibration made on 30 °C and 40 °C isothermal calorimetry does not allow correct prediction of the adiabatic temperature. The kinetic of hydration is stopped around 20 h and the maximal temperature reached is only 75 °C while the other models give around 85–90 °C. This simplified approach can be sufficient if the parameters are identified on a specimen subjected to similar temperature history (isothermal calorimetry for thin structures and adiabatic calorimetry for large ones) but cannot be used to predict very different thermal history than the one used for the fitting.

The other teams (1, 2, 3 and 7) obtained quite similar results. Team3 obtains the lower temperature (between these 4 teams). It comes from the fact that with the affinity law fitted on the isothermal calorimetry, the maximal hydration degree is obtained around 30 h at 60 °C (as it can be seen in Fig. 22). In this adiabatic test, as the temperature quickly reaches values higher than 60 °C, the maximal hydration degree is reached around 20 h and no more heat is released after this date. Team 2 obtain the higher temperature which can be related with the overestimation of the heat release also observed on the calorimetry performed at 60 °C (Fig. 16).

4.2.4. Results of the case study

The results in terms of temperature evolution at 3 defined locations are given in Figs. 18 and 19.

When applied on the cube, Teams 1, 2, 3 and 7 obtained quite exactly the same results. This is not surprising if we note that the calibrations on the intermediate temperatures were very similar (see Fig. 16) and that the boundary conditions were exactly the same. The results are also very close to the experimental measurements.

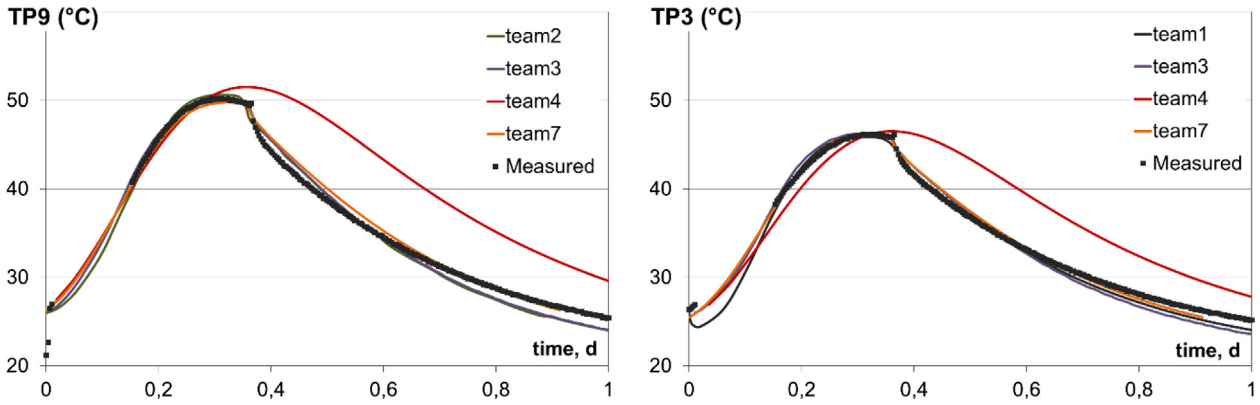

Fig. 19. Surface temperature at mid-height (TP9) and at 5 cm from the bottom face (TP3) from casting to 1 day in a massive concrete cube.

Concerning the results of Team 4 we can see that, contrary to the results on adiabatic test, the temperature obtained here during the heating period (from 0 to 0.4 days) is similar to the one obtained by the other teams. The calibration of their kinetic law on intermediate position between 30 °C and 40 °C seems to compensate here for the fact that a simplified model was used neglecting the activation energy. The main differences are obtained later, during the cooling period, and are due to the fact that the formwork removal was not considered.

4.3. Task 3: modelling development of thermal stress in shrinkage restraining device

4.3.1. General information on modelling approach

All three teams used commercially available software to implement the model for numerical simulation of the benchmark experiment. Detailed information on the modelling approaches are collectively presented in Table 14.

Table 14
Details of numerical simulations of the restraining frame experiment.

	Team 1	Team 2	Team 3
Software used	SOFiSTiK	OOFEM [14]	DIANA
FE idealisation (see Fig. 21)	• regularly meshed 8-node volume elements • thermal boundaries over 2D elements at the surfaces • mechanical boundaries over node supports as well as springs • ¼ of the specimen modelled (double symmetry)		

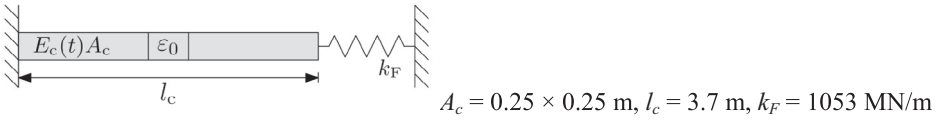

Fig. 20. Idealisation of the restraining frame experiment for mechanical analysis. $A_c = 0.25 \times 0.25$ m, $l_c = 3.7$ m, $k_F = 1053$ MN/m.

Table 15
Parameters for heat generation functions used in simulation of the restraining frame experiment.

Team 1	Team 2	Team 3
$Q_{max} = 104{,}000$ kJ/m^3 $a = -0.8486$ $b = -0.0315$ $\tau_k = 1770$ h	$Q_{pot} = 420$ J/g $B_1 = 0.0002707$ $B_2 = 0.0007$ $\alpha_{max} = 0.85$ $\eta = 6.7$	Adiabatic curve was introduced directly in the model (internal computation of an Arrhenius function inside the processor based on the provided E_a)

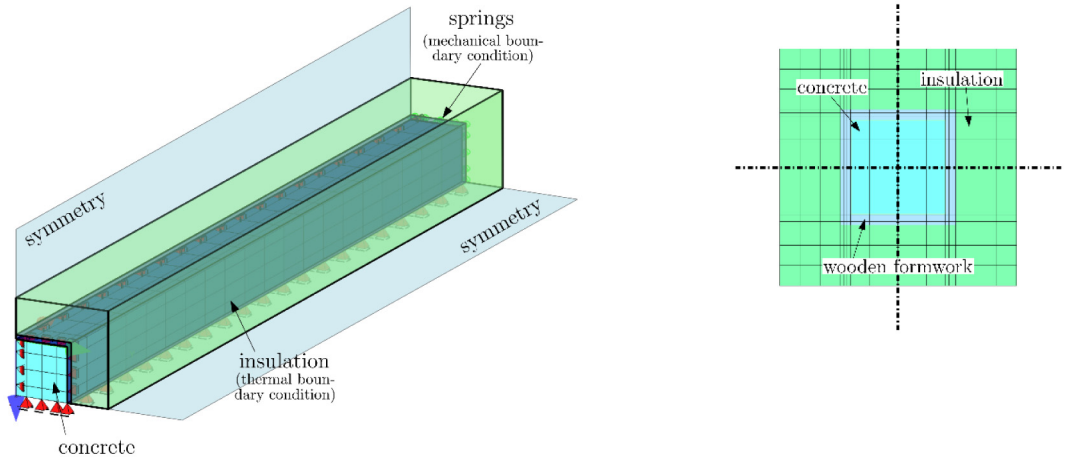

a) 3D view of idealised concrete specimen (1/4 modelled) including mechanical boundaries and schematic illustration of thermal boundaries

b) cross-section for thermal analysis (concrete specimen and covering materials)

Fig. 21. FE model of the restraining frame experiment based on the model of Team 1 (different meshing used by other teams).

The FE models included both concrete specimen as well as formwork and insulation materials for proper simulation of thermal fields. For stress simulation, as ¼ of the specimen was modelled, in the symmetry planes all the surfaces were fixed in normal direction. In the longitudinal direction, one end of the specimen was fixed. whereas at the other end a spring support in the normal direction was introduced with k_F = 1053 MN/m (the value was specified by the frame designer); the scheme is shown in Fig. 20.

4.3.2. Results of thermal analysis

Concrete thermal properties were assumed by all teams as specified in the description. The functions for modelling heat generation were calibrated to fit the provided adiabatic temperature curve. Details are given in Table 15.

Heat transfer coefficient h was taken as specified in the description as well as the ambient temperature T_a which value was equal to 22 °C. Thermal properties of the insulation materials were assumed as specified in the description (Table 6). In symmetry planes adiabatic conditions were considered.

Fig. 22 presents temperature development obtained in simulations of the teams. It must be noted that all teams obtained the maximum temperature to occur earlier than in the experiment. Team 1 was the closest to obtain the maximum temperature value. On the other hand, Team 2 and 3 were able to better simulate the kinetics of the process (heating phase). However, cooling of the specimen began too early and the maximum temperature was underestimated. What must be emphasised is that the drop of temperature due to formwork removal has been well detected by all teams. It can be said that the temperature development was reproduced on a satisfactory level. The deviations of temperature in the range of 0.2–2.5 °C are acceptable given the actual precision of measurements – temperature sensors may easily have deviations of 1–2 °C.

The importance of discrete modelling of insulation for a specimen of such a small cross-section was revealed in preliminary simulations. Initially, the presence of insulation was modelled by introduction of a reduced value of the heat exchange coefficient (which value was computed to be h = 0.5 W/(m^2·K)). As it can be noticed in the diagram in Fig. 23, which presents the results of such simulation made by Team 1, the temperatures obtained in simulations are much higher than in reality. The reason is the significance of heat storage in the formwork and insulation in the present case, where the temperatures in the interior are significantly affected by the surface conditions – even if the simulated temperature history is comparable to thick members. In the beginning of the warming phase additional losses due to the outflow of heat into the formwork and insulation system occur according to the temperature of the specimen. Moreover, the temperature history at the temperature maximum is somewhat delayed due to the stored heat in formwork and insulation. A realistic simulation of both requires a discrete modelling of formwork as well as insulation with additional elements.

4.3.3. Results of stress analysis

Thermal strains were computed with the specified value of coefficient of thermal dilation $\alpha_T = 10 \cdot 10^{-6}$. Shrinkage strains

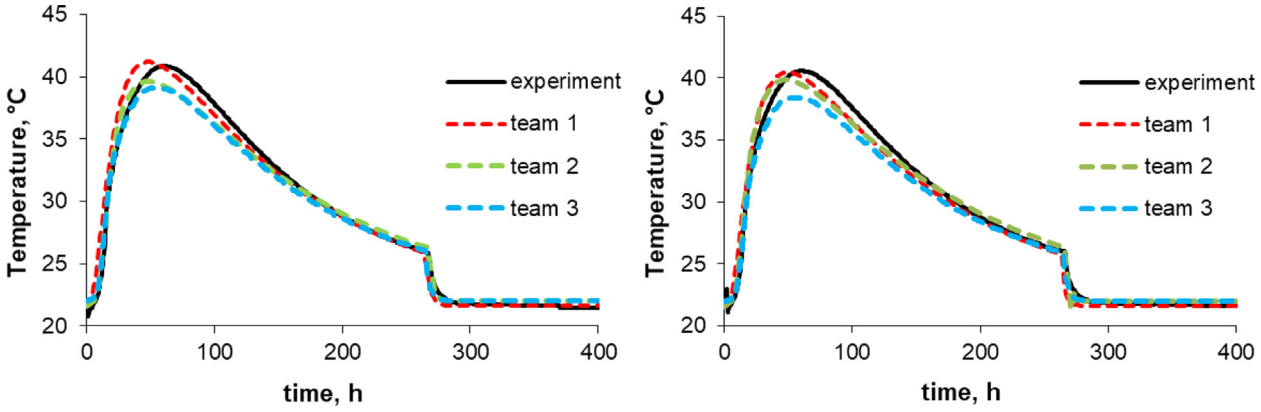

Fig. 22. Simulation of temperature development (left) in the core and (right) in the corner of the specimen in the restraining frame experiment.

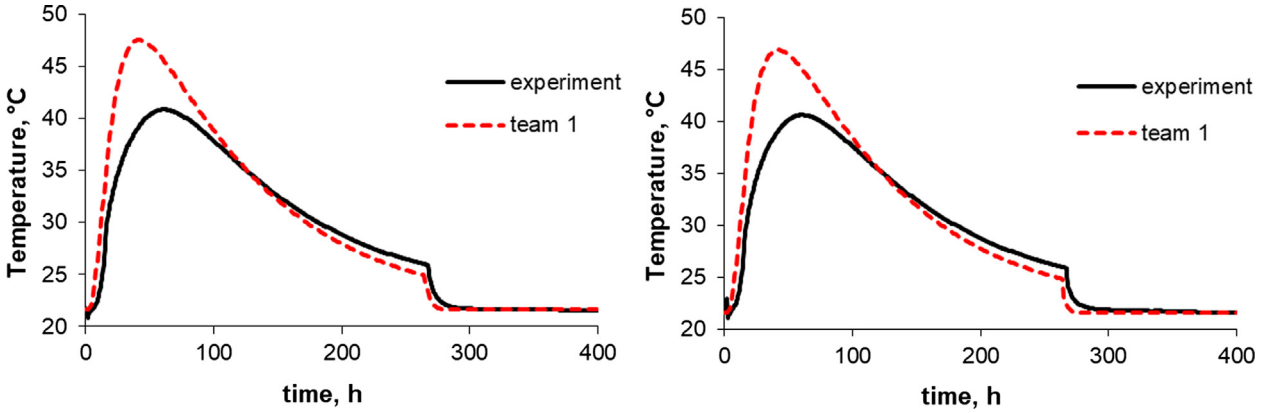

Fig. 23. Overestimation of temperature development (left) in the core and (right) in the corner of the specimen in simulation of the restraining frame experiment due to application of simplified boundary conditions.

were computed with the ultimate value of $\varepsilon_{ca,\infty} = 0.05$ and time-development as specified in Table 16.

Stress development was determined with viscoelastic models. Detailed information about the applied values of the Young modulus and creep functions are given in Table 16.

Fig. 25 presents average stress development in the simulated restrained specimen. The best compliance was achieved by Team 1. Comparatively good results were obtained by Team 2, especially concerning the level of compressive stresses and tensile stresses while in formwork. The stresses in a member after formwork removal are, however, overestimated, which is also the case for Team 3. Comparing the results of elastic calculations, which are not affected by the creep model used, it appears that the obtained results are very similar. The differences most probably results from the differences in the values of thermal and shrinkage strains as well as in the Young modulus development – these discrepancies superpose during the modelling process. Nevertheless, it is evident that the applied creep function and calibration of its parameters

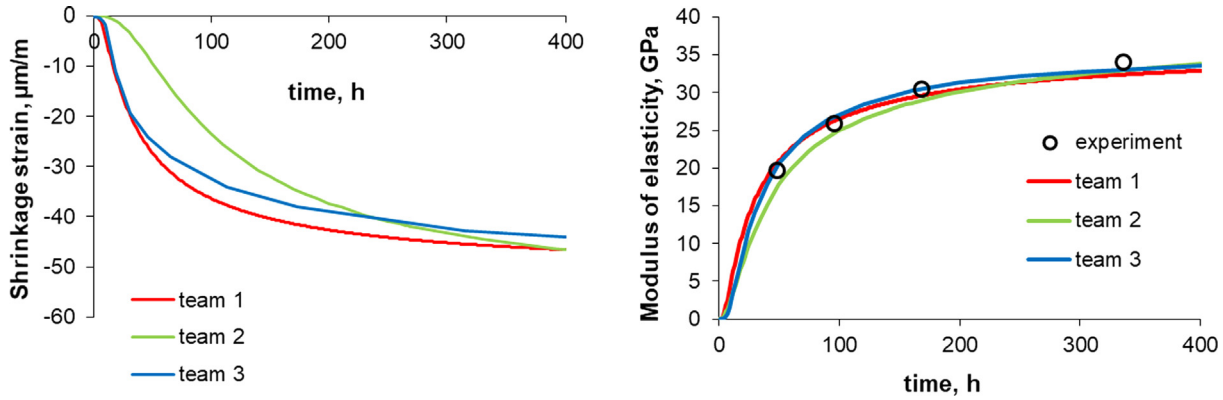

Fig. 24. Autogenous shrinkage strain (left) and Young modulus (right) development applied in simulation of the restraining frame experiment.

Table 16
Parameters for mechanical models for simulation of the restraining frame experiment.

Team 1	Team 2	Team 3
Shrinkage strain (see Fig. 24 left)		
a, b and τ_k as in Table 15. $\alpha_{max} = 0.95$	Shrinkage development related to equivalent age and material composition w/c $\alpha_{max} = 0.85$	Linear relation between the hydration degree and shrinkage with ε_{ca} (α=1) = 0.5‰
Young modulus (see Fig. 24 right)		
$a \cdot w/c = 6.25 \cdot 0.48 = 3.0$ $\beta_{wes} = -0.8$	The parameters of B3 model for basic creep $q1$-$q4$ are estimated from the composition of concrete mixture and compressive strength (f_c, w/c, a/c)	Measured values directly implemented
Creep		
RH = 60% h_0 = 12.5 cm	sealed conditions	RH = 60% h_0 = 12.5 cm

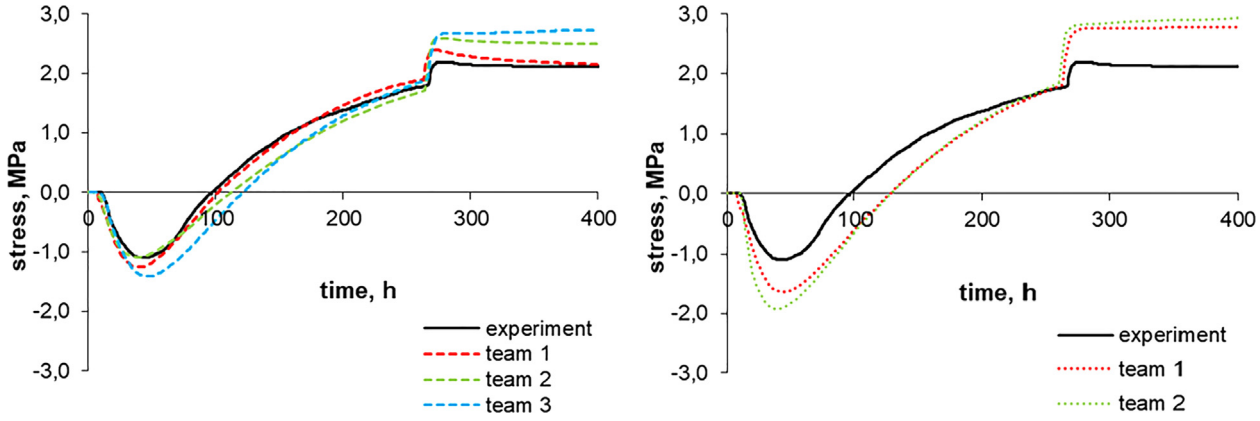

Fig. 25. Simulation of viscoelastic (left) and elastic (right) stress development in the restraining frame experiment.

has the most significant influence on the values of stresses obtained in numerical simulation.

5. Conclusions

The following conclusions can be drawn from this stage of the benchmark program:

5.1. Conclusions concerning prediction of thermal behaviour

1. As it was expected, tasks 1 and 2 confirmed that it is crucial to consider the activation energy while simulating the temperature evolutions in concrete at early ages. It was shown that even if the activation energy (used to simulate this thermal activation) slightly differs (14% for task 2), the combined identification of E_a and the affinity leads to good prediction of temperature evolution in thermal conditions which can be slightly different from the ones used to identify model's parameters (this was observed also in [31]). Some differences can appear in the case of the simulation of adiabatic temperature rise with models identified on isothermal calorimetry (task 2) but they are linked to the a misprediction of the final hydration degree (that is obtained too soon in some cases).
2. Tasks 2 and 3 also confirmed that the good reproduction of the surface temperatures is highly conditioned by a precise modelling of the boundary conditions. In particular it was shown that in the case of thin formwork with no insulation (task 2), an equivalent is sufficient to model the effect of formwork. But in the case of an important insulation (task 3), the satisfactory simulation of temperature history requires discrete modelling of formwork and insulation with additional FE elements. This is due to the significance of heat storage in these thick insulation materials compared to the heat storage of the rather thin cross-section of the specimen.

5.2. Conclusions concerning prediction of mechanical behaviour

1. Comparison of early-age stresses showed differences even in elastic analysis (it was especially visible in task 1). This was caused by inaccurate reproduction of Young modulus and autogenous shrinkage development; setting, kinetic and amplitude of these material properties should be predicted precisely. It is also crucial to take into account in modelling that stiffness of the material only starts to develop after setting, otherwise the initial compressive stresses are overestimated which affects further stress history.
2. As it was expected, creep had an important influence on the magnitude of early-age stresses and even higher differences were observed in viscoelastic analysis (task 3). What can be concluded from this stage of benchmark is that creep is still one of the biggest challenges in modelling of early-age concrete. It was shown that even though the models used in this benchmark were validated and can reproduce experimental measurements if a complete set of data is known, prediction of stresses is still a challenge.

Acknowledgments

The authors would like to acknowledge networking support by the COST Action TU1404 (www.tu1404.eu).

Funding sources

In the particular case of the team members at the University of Minho (Portugal), his work was also partially financed by FEDER funds through the Competitivity Factors Operational Programme – COMPETE and by Portuguese national funds through FCT – Foundation for Science and Technology within the scope of the projects POCI-01-0145-FEDER-007633 and POCI-01-0145-FEDER-016841 (PTDC/ECM-EST/1056/2014).

In the particular case of the leading author, her work was also partially financed by the funds of the Polish Ministry of Science and Higher Education (BK-237/RB-6/2018).

References

[1] COST Action TU 1404, http://www.tu1404.eu/ (accessed on 18 Nov 2017).
[2] EDF Vercors 2018 benchmark https://fr.xing-events.com/EDF-vercors-project.html (accessed on 18 Nov 2017).
[3] L. Buffo-Lacarrière, A. Knoppik-Wróbel, Objectives and plan of the group priority GP2e, Benchmarking calculations, COST TU1404 Workshop, Vienna, Austria, 2015 (electronic access: https://zenodo.org/record/46070).
[4] RRT+: Main phase of the Extended Round Robin Testing programme for TU1404. Testing protocols, 2016 (electronic access: http://www.tu1404.eu/wp-content/uploads/2017/12/RRT-Main-phase_Protocols_06112017.pdf).
[5] A.D. Cameron, J.A. Casey, G.B. Simpson, Benchmark test for thermal analysis (Summary Report), NAFEMS, 1986.
[6] M. Wyrzykowski, J. Sanahuja, L. Charpin, M. Königsberger, Ch. Hellmich, B. Pichler, L. Valentini, T. Honório, V. Smilauer, K. Hajkova, G. Ye, P. Gao, C. Dunant, A. Hilaire, S. Bishnoi, M. Azenha, Numerical benchmark campaign of COST Action TU1404 – microstructural modelling, RILEM Tech. Lett. 2 (2017) 99–107.
[7] F. Benboudjema, A. Knoppik, L. Lacarrière, M. Wyrzykowski, Modeling of concrete at early age – benchmark carried out within COST TU 1404, Proc. JCI-RILEM International Workshop on "Control of Cracking of Mass Concrete and Related Issues Concerning Early Age Cracking of Concrete Structures" CONCRACK5, Tokyo, Japan, 2017.
[8] M. Azenha, R. Faria, H. Figueiras, Thermography as a technique for monitoring early age temperatures of hardening concrete, Constr. Build. Mater. 25 (2011) 4232–4240.
[9] K. Turner, D. Schlick, N.V. Tue, Restraint and crack width development during service life regarding hardening caused stresses, Proc. fib Symposium, Copenhagen, Denmark, 2015.
[10] W. Hermerschmidt, Modelle zur Beschreibung der thermomechanischen Materialeigenschaften jungen Betons PhD Thesis, TU Braunschweig, 2016.
[11] H. Freiesleben, P. Hansen, E.J. Pedersen, Maleinstrument til Kontrol af befons haerding, Nordisk Beton 1 (1977) 21–25.
[12] J.E. Jonasson, Modelling of Temperature, Moisture and Stresses in Young Concrete PhD Thesis, Lulea University of Technology, 1994.
[13] R. Poulsen, M. Christiansen, Numerisk simulering af temperatur- og spændingstilstanden i hærdnende betonkonstruktioner Master Thesis, Aalborg Universitet, 2009.
[14] V. Šmilauer, L. Baquerizo, T. Matschei, P. Havlásek, W. Leal Da Silva, K. Hájková, ConTemp – A virtual thermo-mechanical simulator for hydrating reinforced concrete blocks with extension to service life, Proc. Service Life of Cement-Based Materials and Structures. Lyngby, Denmark, 2016.
[15] L. Buffo-Lacarrière, A. Sellier, G. Escadeillas, A. Turatsinze, Multiphasic finite element modelling of concrete hydration, Cement and Concrete Res. 37 (2) (2007) 131–138.
[16] H. Reinhardt, J. Blaauwendraad, J. Jongedijk, Temperature development in concrete structures taking account of state dependent properties, Proc. International Conference of Concrete at Early Ages, Paris, France, 1982.
[17] V. Troyan, Prediction of crack resistance of massive concrete structures based on cements different types, Modern Tech. Technol. 2 (2015) (electronic journal).
[18] G. Sciumè, F. Benboudjema, C. De Sa, F. Pesavento, Y. Berthaud, B.A. Schrefler, A multiphysics model for concrete at early age applied to repairs problems, Eng. Struct. 57 (2013) 374–387.
[19] K. Wesche, Baustoffe für tragende Bauteile, Band 2: Beton und Mauerwerk, Vieweg + Teubner Verlag, 1993.
[20] D. Schlicke, Mindestbewehrung zwangbeanspruchter Betonbauteile unter Berücksichtigung der erhärtungsbedingten Spannungsgeschichte und der Bauteilgeometrie PhD Thesis, TU Graz, 2014.
[21] fib Model Code for Concrete Structures 2010.
[22] Z.P. Bažant, S. Baweja, Creep and Shrinkage Prediction Model for Analysis and Design of Concrete Structures: Model B3, Technical Report, American Concrete Institute, 2000.
[23] G. de Schutter, Degree of hydration based Kelvin model for the basic creep of early age concrete, Mater. Struct. 32 (1999) 260–265.
[24] L. Granger, Comportement différée du béton dans les enceintes de centrale nucléaire: analyse et modélisation PhD Thesis, ENPC, 1995.

[25] A. Hilaire, F. Benboudjema, A. Darquennes, Y. Berthaud, G. Nahas, Modeling basic creep in concrete at early-age under compressive and tensile loading, Nucl. Eng. Des. 269 (2014) 222–230.
[26] E. Strieder, R. Hilber, R. Murr, K. Bergmeister, Entwicklung der Materialeigenschaften im jungen Massenbeton, Beton-Stahlbetonbau 112 (1) (2017) 41–49.
[27] L. Nietner, D. Schlicke, N.V. Tue, Berücksichtigung von Viskoelastizität bei der Beurteilung von Zwangbeanspruchungen erhärtender Massenbetonbauteile, Beton-Stahlbetonbau 106 (3) (2011) 169–177.
[28] F. Benboudjema, J.M. Torrenti, Early age behaviour of concrete nuclear containments, Nucl. Eng. Des. 238 (10) (2008) 2495–2506.
[29] J.L. Tailhan, L. D'Aloia, P. Autuori, Simulations numériques du comportement au jeune âge des structures en béton: modélisation et retour d'expérience, BLPC 278 (2010) 65–77.
[30] L. Buffo-Lacarrière, A. Sellier, B. Kolani, B., Application of thermo-hydro-chemo-mechanical model for early age behaviour of concrete to experimental massive reinforced structures with strain-restraining system, Eur. J. Environ. Civ. Eng. 18 (7) (2014) 814–827.
[31] M. Briffaut, F. Benboudjema, J.M. Torrenti, G. Nahas, Analysis of semi-adiabiatic tests for the prediction of early-age behavior of massive concrete structures, Cem. Concr. Comp. 34 (5) (2012) 634–641.